IOP Publishing Smart Materials and Structures
Smart Mater. Struct. **32** (2023) 065002 (16pp) https://doi.org/10.1088/1361-665X/accb21

Electric resistivity evolution in NiTi alloys under thermomechanical loading: phase proportioning, elasticity and plasticity effects

Marcos Lopes Leal Júnior[1,2,3,*], Laurent Pino[1], Mahmoud Barati[2,3,4], Luc Saint-Sulpice[1], Laurent Daniel[2,3] and Shabnam Arbab Chirani[1]

[1] ENI Brest, UMR CNRS 6027, IRDL, F-29200 Brest, France
[2] Université Paris-Saclay, CentraleSupélec, CNRS, Laboratoire de Génie Électrique et Électronique de Paris, 91192 Gif-sur-Yvette, France
[3] Sorbonne Université, CNRS, Laboratoire de Génie Électrique et Électronique de Paris, 75252 Paris, France
[4] Institut Polytechnique des Sciences Avancées, IPSA, 94200 Ivry-sur-Seine, France

E-mail: lopes@enib.fr

Received 15 December 2022, revised 1 April 2023
Accepted for publication 6 April 2023
Published 21 April 2023

Abstract

The well-known martensitic transformation is the main feature for almost all shape memory alloys (SMAs) usage. Meanwhile, the practical implementation of SMA in devices is not straightforward due to the evolution of their functional properties in operation. This evolution is mainly due to the different interactions between the martensite transformation (MT) or detwinning and mechanisms such as plasticity. Although these mechanisms are extensively studied by fine and precise techniques (e.g. high energy x-ray diffraction and transmission electron microscopy), their impact on a macroscopic level (usage scale) are not fully clarified. In this work, the effects of some of the most influential mechanisms in a NiTi alloy are investigated by using electric resistivity measurements at macroscopic scale. Distinct phase proportioning approaches are employed to analyze the martensitic transformation kinetic. It is found that, unlike elastic strains, plastic strains are a key influential factor on resistivity variations in SMAs. It is also shown that the use of an assumption of linearity between fraction of stress-induced martensite and strain transformation can lead to unrealistic interpretations of transformation mechanisms in NiTi wires.

Keywords: SMA, NiTi, martensite transformation, electric resistivity, plasticity, phase proportioning, phase transformation kinetics

(Some figures may appear in colour only in the online journal)

* Author to whom any correspondence should be addressed.

1. Introduction

Shape memory alloy (SMA) wires exhibit impressive behaviors, such as superelasticity, pseudoplasticity and shape memory effect under thermomechanical loading. These features are triggered by shear lattice distortion, a diffusionless process known as martensitic transformation (MT) that occurs between a parent austenite and a product martensite crystal structures. Such peculiar characteristics are very useful in various industry applications. Among the different options of SMA composition, the NiTi alloys are the most employed due to their steadier behavior upon cyclic use and their wide range of operating conditions when compared to others SMAs [1, 2].

However, one of the main drawbacks for the usage of SMAs in engineering applications is the evolution of thermomechanical response upon cycling (also denoted as functional fatigue). This shortcoming makes it difficult to accurately design and control SMA-based devices in industry [3, 4].

Among the major actors of the evolution of the properties of SMAs, the interactions between phase transformation and plasticity are the most significant. These interactions take place at the microstructural level and impact directly the macroscopic behavior. In some cases, where the microstructure is more complex compared to others SMAs, as for NiTi alloys, this relation can be even more pronounced.

Being the most influential mechanism, the coupling between phase transformation and plasticity can occur in two different ways: upon repeated loading and under conditions that exceed the elastic domain. In the first case, the propagation of austenite/martensite interfaces results in lattice defects (mainly composed of slip dislocations (plasticity)) and residual stress-induced martensite (initiated due to internal stress accumulation) [5–7]. Then, the effects of the interactions are gradually accumulated, leading to a degradation of the functional properties. In the second case, plastic effects are more intense and complex. In some works [8–11], the authors investigated this phenomenon and analyzed the evolution of different parameters during high stress experiments. It was highlighted that for temperatures much higher than A_f, dislocation slip can occur during transformation, resulting in a considerable amount of unrecoverable deformation and changing considerably the kinetics of MT or detwinning (DT).

Therefore, the understanding of phase transformation (MT and DT) kinetics and its interactions with other mechanisms become a key-factor to the design of SMA-based devices. But despite the large amount of studies on these mechanisms, very few studied its impact on a macroscopic scale, which is the scale of usage.

The understanding of the aforementioned mechanisms is also fundamental for modeling aspects. Presently, several modeling strategies can be employed to simulate the behavior of SMAs. The models can be defined at micro, micro–macro and macroscopic scales. Typically, in micro and micro–macro approaches (extensively detailed models), the phenomena are treated at the grain/crystal or lattice particles levels. Its modeling is mostly based on the Ginzburg–Landau theory or on molecular dynamics and the description of effects such as nucleation or interface motion are often implemented [12–15]. On the other hand, for macroscopic approaches, phenomenological considerations and experimental fitting are employed to determine the interactions between the most influential mechanisms and its kinetics.

Different investigation methods are employed to analyze the kinetics and interactions at different scale levels. The most implemented techniques are the observations of the microstructure by transmission electron microscopy (TEM) [5, 6, 9, 16], high-energy x-ray diffraction [5, 8] or *in-situ* electric resistivity [17–21]. The amount of data provided by each of these methods varies a lot, as well as the cost of their usage. While x-ray diffraction and TEM analysis contribute with precise and fine resolution images of the microstructure and its rearrangement, electric resistivity measurements provide the user with real-time microstructural state response in a more approachable way.

The purpose of the present work is to analyze the kinetics of the phase transformation for a NiTi wire and some of its main interaction mechanisms at a macroscopic level (usage scale). The experiments are performed by employing electric resistivity measurement under different thermomechanical loading paths. The impact of elastic and plastic strain interactions during phase transformation is determined by using two phase proportioning techniques implemented in a macroscopic approach. Is worth mentioning that, in most of the similar studies, the effect of elastic and plastic strain components are not considered [19, 22–25].

Furthermore, the validity of the most employed relation to the description of the kinetics of MT/DT (a linear correspondence between the volume fraction of the stress-induced martensite and the transformation strain component [18, 26]) is also evaluated through the comparison of two different microstructural states.

2. Materials and experimental procedures

2.1. Studied materials

In this study, two NiTi wires have been considered. The first is a 0.51 mm diameter NiTi equiatomic wire produced by Dynalloy® and the second is a 0.39 mm diameter wire produced by Fort Wayne Metals® (graded as #6).

The Dynalloy wire (DN) is designed to actuation end and shows two-way shape memory effect (TWSME). The most common procedure used to provide this property to SMAs is the training [17, 27–31]. The Fort Wayne Metals® wire (FW) does not show TWSME, it is also indicated to actuation usage.

First, phase transformation temperatures M_s, M_f, A_s, A_f, R_s and R_f of both wires were determined by differential scanning calorimetry (DSC) in order to set the temperature conditions for testing. These parameters indicate at which temperature the forward phase transformation and reverse phase transformation starts (temperatures with subscripts '*s*') and finishes (subscripts '*f*') in a stress-free condition. In some cases, an intermediate phase, the *R*-phase (rhombohedral) is also present in the material and it is denoted by $R_{s/f}$. All transformation temperatures are presented in figure 1. In order to identify the mechanical and the electrical response of the NiTi wires,

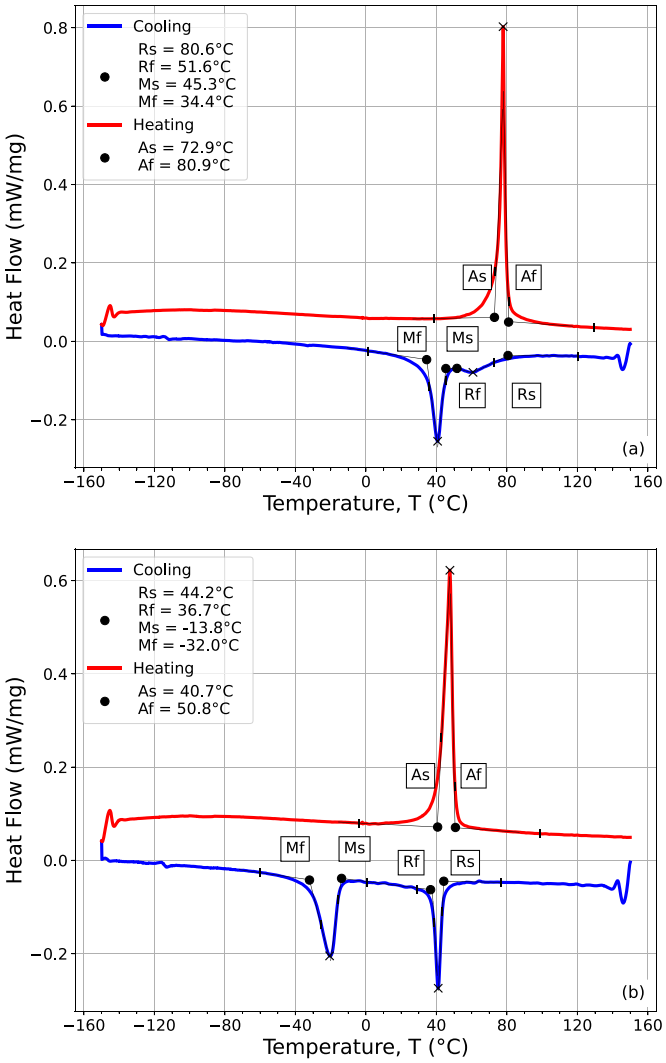

Figure 1. DSC test for DN (a) and FW (b) wires.

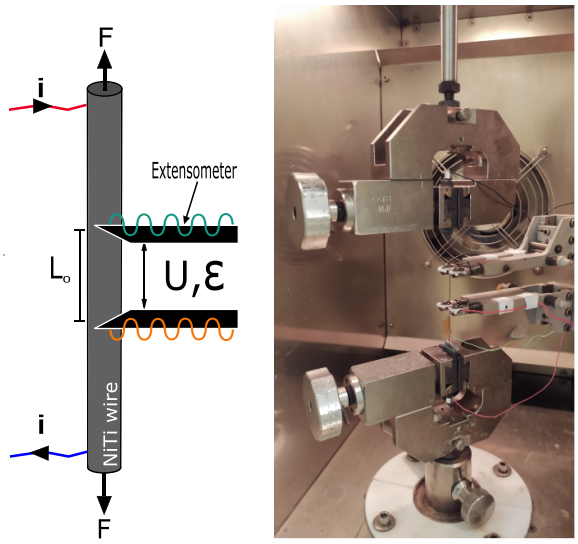

(a) Four-wire lead measurement method. (b) Experimental setup.

Figure 2. Experimental setup for voltage variation measurement.

thermomechanical tests were performed with displacement, force and electric voltage measurements. In these tests, the two different commercial wires were used.

2.2. Experimental conditions

The thermomechanical experiments were performed using a Zwick electromechanical testing machine (Zwick Z050) equipped with an extensometer to measure the axial strain ε, with a thermal chamber (Zwick BW91250) to control the temperature T surrounding the specimen and with a 500 N load cell to determine the axial stress σ.

Two different loading paths were used to analyze the behavior of the wires: isothermal tests were performed to investigate the superelastic (SE) and pseudoplastic (PP) behaviors, while anisothermal tests investigate the shape memory effect.

For isothermal loading, a low strain rate of $10^{-4}\,\mathrm{s}^{-1}$ was set, whereas for anisothermal ones, a temperature rate of $\pm 4\,^{\circ}\mathrm{C\,min}^{-1}$ was imposed. In both types of loading, the temperature was measured by a K-type thermocouple placed on the specimen and a four-wire lead measurement method was used to feed the specimen with DC current and to record the voltage variation between extensometers as shown in figure 2(a). This method consists in applying a low constant electric current between the ends of the wire and in measuring the resulting electric voltage between the pair of extensometer arms. For this, the specimen needs to be electrically isolated from the testing machine and from the extensometer to avoid external noise (see figure 2(b)). The resulting voltage is used to calculate the resistivity of the specimen during testing (see next section).

2.3. Resistivity analysis

By adopting the same procedure as in [32], it is possible to calculate the voltage variation during thermomechanical loading. The voltage variation is linked to phase transformations and to the geometrical changing of the specimen during testing. Equation (1) shows that the specimen's electric resistance is a function of the electric resistivity of the material, geometrical characteristics and axial strain when the volume of the specimen is considered constant

$$R = \frac{L^2}{V_0}\rho = \frac{(L_0(1+\varepsilon))^2}{V_0}\rho, \tag{1}$$

$$\Delta R = \frac{2L}{V_0}\rho\Delta L + \frac{L^2}{V_0}\Delta\rho, \tag{2}$$

where R is the electric resistance, L the length, V the volume, ρ the total resistivity and ε the strain of the wire. The subscript '0' indicates the initial value of each parameter.

By differentiating this equation and using the relation equation (3), the connection between the voltage variation and the two major contributing factors are demonstrated in equations (5) and (6)

$$\Delta U = i\Delta R, \tag{3}$$

$$\Delta U = U_0 \frac{\Delta R}{R_0} = U_0 \left(\frac{\Delta R_\varepsilon}{R_0} + \frac{\Delta R_\rho}{R_0} \right), \tag{4}$$

$$\Delta U_\rho = U_0 \frac{\Delta R_\rho}{R_0} = U_0 (1+\varepsilon)^2 \frac{\Delta \rho}{\rho_0}, \tag{5}$$

$$\Delta U_\varepsilon = U_0 \frac{\Delta R_\varepsilon}{R_0} = 2U_0 (1+\varepsilon)\varepsilon. \tag{6}$$

In this study, only the resistivity related to the phase transformation electric voltage (ΔU_ρ) is analyzed and the final expression for the resistivity measurement is then presented in equation (7)

$$\rho = \rho_0 \left(1 + \frac{\Delta U_\rho}{U_0 (1+\varepsilon)^2} \right). \tag{7}$$

The electric resistivity itself can be written as a function of the electric resistivity of each pure state present in the material, volume fraction of the states and the temperature as

$$\rho = \rho \left(\rho_A, \rho_{M^T}, \rho_{M^\sigma}, \rho_R, z_A, z_{M^T}, z_{M^\sigma}, z_R, T \right), \tag{8}$$

where the subscripts A, M^T, M^σ and R are used to indicate the resistivity (ρ_i) and volume fraction (z_i) of the austenite, thermally-induced martensite, stress-induced martensite and R-phase, respectively. In this work, all the R-phase components will not be considered in the analysis (ρ_R and $z_R = 0$), since their appearance does not occur on the different loading paths considered here [29, 33, 34].

Therefore, each of the others remaining pure states (A, M^T and M^σ) may be considered a function of temperature, elastic and plastic strain [17, 32], as

$$\rho_i = \rho_i(T, \varepsilon^{\text{el}}, \varepsilon^p), \tag{9}$$

by differentiating this equation, the following can be obtained,

$$\Delta \rho_i = \frac{\partial \rho_i}{\partial T} \Delta T + \frac{\partial \rho_i}{\partial \varepsilon^{\text{el}}} \Delta \varepsilon^{\text{el}} + \frac{\partial \rho_i}{\partial \varepsilon^p} \Delta \varepsilon^p. \tag{10}$$

In this equation, one can observe the possible contribution of three different mechanisms on the variation of the resistivity of a pure state.

Finally, by using the serial mixture-law in conjunction with condition that the sum of all volume fractions is equal to one, the resistivity relationship is given by:

$$\rho = (1 - z_{M^T} - z_{M^\sigma}) \rho_A + z_{M^T} \rho_{M^T} + z_{M^\sigma} \rho_{M^\sigma}. \tag{11}$$

In the next sections, two different techniques of phase proportioning based on resistivity measurements are presented. These approaches will be essential to clarify the influence of the strain and temperature components on the resistivity response.

2.4. Two-state phase proportioning post processing

In order to study the MT kinetics and the volume fraction of the different states during thermomechanical loading, a two-state phase proportioning method based on the electric resistivity variation is implemented [18]. For this approach, only the thermomechanical loading paths that one single state/phase transformation follows can be analyzed ($A \longleftrightarrow M^\sigma$ or $M^T \longrightarrow M^\sigma$). In this case, the total resistivity of the material is calculated by the following relation:

$$\rho(T) = (1 - z_{M^\sigma}) \rho_l(T) + z_{M^\sigma} \rho_{M^\sigma}(T), \tag{12}$$

where l represents M^T or A state. The resistivity of each pure phase/state (ρ_i, with $i = M^\sigma, M^T$ or A) is considered to be temperature-dependent only (the change in resistivity due to elastic and plastic deformations is not accounted for):

$$\rho_i(T) = \mu_i T + \rho_i^0, \tag{13}$$

where μ_i is the slope of electric resistivity response, corresponding to $\partial \rho_i / \partial T$ and the strain components are zero ($\partial \rho_i / \partial \varepsilon^{el}$ and $\partial \rho_i / \partial \varepsilon^p = 0$) and ρ_i^0 is the reference electric resistivity value at 0 °C.

By rearranging the elements in equation (12), the volume fraction of each state ($A + M^\sigma$ or $M^T + M^\sigma$) is then given by:

$$z_{M^\sigma} = \frac{\rho(T) - \rho_l(T)}{\rho_{M^\sigma}(T) - \rho_l(T)}, \tag{14}$$

$$z_l = 1 - z_{M^\sigma}. \tag{15}$$

Thus, by measuring the temperature and the resistivity during loading and by using the resistivity of pure phases/states, it is possible to determine the volume fraction of each state/phase during certain loading paths.

2.5. Three-state phase proportioning post processing

For more complex loading paths, in which three different states can be present, another approach is proposed. The adopted method is the same as the one developed by [17], for a CuAlBe SMA. In this post processing, the effective elastic modulus (E) and the resistivity (ρ) are dependent on the volume fraction of each state. The effect of the plastic strain is not considered, then the total strain can be decomposed into three components (elastic, transformation and thermal), as shown in equation (16)

$$\varepsilon = \varepsilon^{\text{el}} + \varepsilon^{\text{tr}} + \varepsilon^{\text{th}}. \tag{16}$$

The strain components are calculated as,

$$\varepsilon^{\text{el}} = \frac{\sigma}{E(z_{M^\sigma}, z_{M^T}, z_A)}, \tag{17}$$

$$\varepsilon^{\text{th}} = \alpha (T - T_0), \tag{18}$$

where σ, is the nominal stress, α is the thermal expansion coefficient and T_0 is the reference temperature. To evaluate the

transformation strain, a supplementary equation is necessary. The relation between the volume fraction of stress-induced martensite and the transformation strain (equation (19)), proposed by [26, 35, 36] is adopted. This relation assumes that the evolution of stress-induced martensite volume fraction is proportional to the transformation strain, as shown in the experiment of [18], performed on a CuAlBe alloy

$$z_{M^\sigma} = \frac{\varepsilon^{\mathrm{tr}}}{\gamma}. \tag{19}$$

The parameter γ corresponds to the maximum transformation strain.

In this approach, the resistivity evolution of each pure state is also considered as temperature-dependent only (equation (13)), as in the previous post processing technique.

Finally, the transformation strain and the volume fraction of each of the three states are estimated by using equations (20)–(24):

$$\sigma = (a + b\varepsilon^{\mathrm{tr}})(\varepsilon - \varepsilon^{\mathrm{el}} - \varepsilon^{\mathrm{th}}), \tag{20}$$

where σ corresponds to mechanical stress and a and b terms to:

$$a = \left(1 - \frac{\rho - \rho_A}{\rho_{M^T} - \rho_A}\right) E_A + \left(\frac{\rho - \rho_A}{\rho_{M^T} - \rho_A}\right) E_M, \tag{21}$$

$$b = \left(1 - \frac{\rho_{M^\sigma} - \rho_A}{\rho_{M^T} - \rho_A}\right) \frac{E_M - E_A}{\gamma}, \tag{22}$$

where E_M and E_A are the elastic moduli of the martensite (considered the same for thermally-induced and stress-induced martensite) and austenite, respectively. The transformation strain is given by:

$$\varepsilon^{\mathrm{tr}} = \frac{\sqrt{(a - b(\varepsilon - \varepsilon^{\mathrm{th}})^2 - 4b(\sigma - a(\varepsilon - \varepsilon^{\mathrm{th}}))}}{2b} - \frac{(a - (b(\varepsilon - \varepsilon^{\mathrm{th}}))}{2b}, \tag{23}$$

and the volume fraction of each state is calculated as:

$$z_{M^T} = \frac{\rho - \rho_A}{\rho_{M^T} - \rho_A} - \frac{\varepsilon^{\mathrm{tr}}}{\gamma} \frac{\rho_{M^\sigma} - \rho_A}{\rho_{M^T} - \rho_A}, \tag{24}$$

$$z_A = 1 - z_{M^T} - z_{M^\sigma}. \tag{25}$$

3. Results and discussion

3.1. Identification of material parameters

Given the experimental procedure, the aim of this section is to identify the material parameter values needed for the phase proportioning. First, in order to collect the standard characteristics of pure phases, different tests were realized and the identified parameters values are presented in tables 1 and 2.

The elastic moduli and the γ parameter were extracted from SE tests at different temperatures and in different phases (figures 3(a) and 4(a)). Additional material parameters and the phase diagrams are presented in figures 5 and 6. Then, the electric properties μ and ρ_0 were extracted from shape memory effects tests at different stress levels (figures 7 and 8) and by considering that the evolution of the resistivity of a pure phase is a linear function of the temperature as in equation (13).

Table 1. DN wire properties.

Phase state	E (GPa)	γ (%)	$\mu \times 10^{-9}$ (Ω.m K^{-1})	$\rho_0 \times 10^{-7}$ (Ω.m)
M^σ	44.6	6.5	1.34	7.07
M^T			1.34	7.69
A	80.9		0.34	6.88

Table 2. FW wire properties.

Phase state	E (GPa)	γ (%)	$\mu \times 10^{-9}$ (Ω.m K^{-1})	$\rho_0 \times 10^{-7}$ (Ω.m)
M^σ	45.2	6.7	1.39	8.66
M^T			1.08	7.35
A	82.9		0.29	7.34

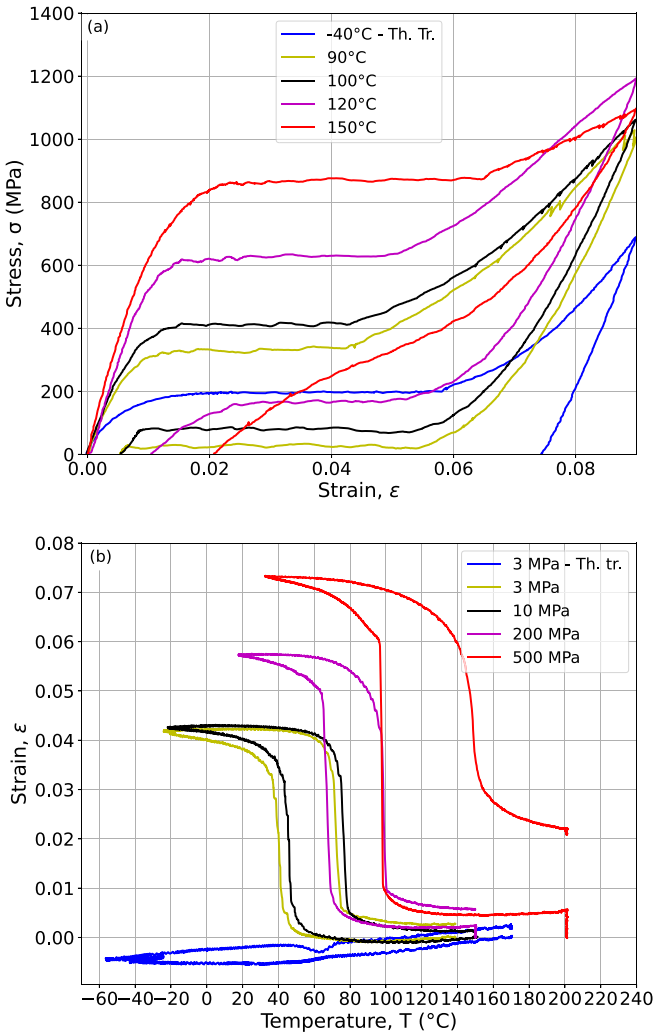

Figure 3. SE/PP (a) and SME (b) tests for DN wires.

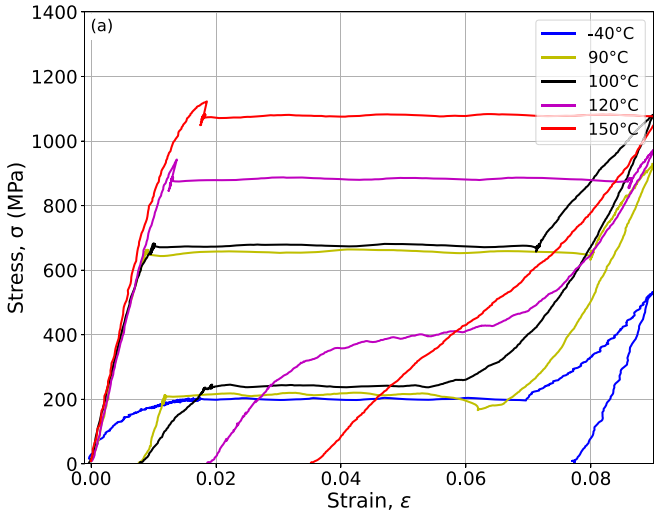

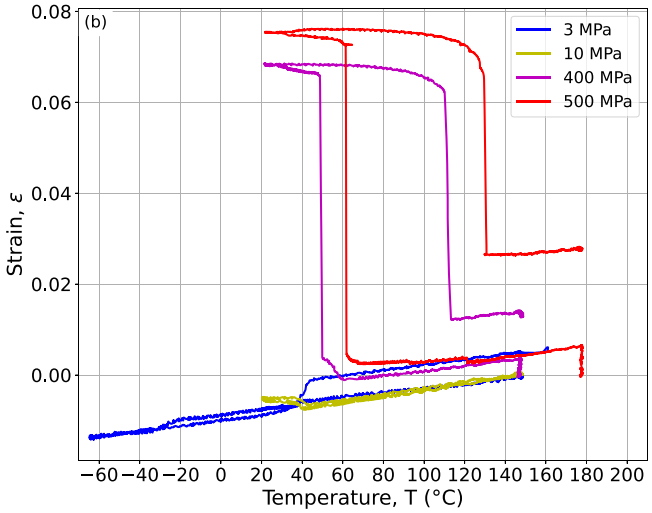

Figure 4. SE/PP (a) and SME (b) tests for FW wires.

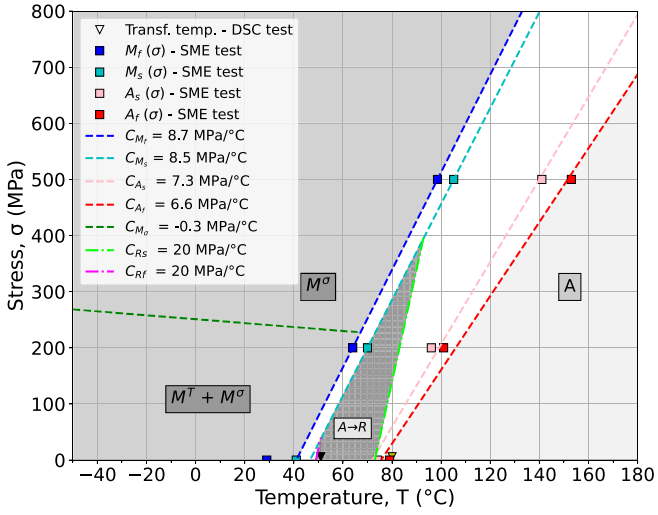

Figure 5. DN phase diagram.

The resistivity diagram of each wire are shown in figures 7 and 8. The curves represent the evolution of electric resistivity at different levels of loading. Each linear stage, corresponds to

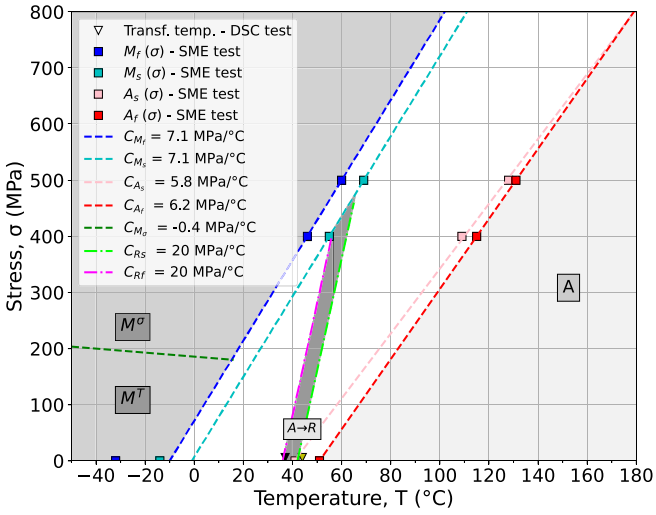

Figure 6. FW phase diagram.

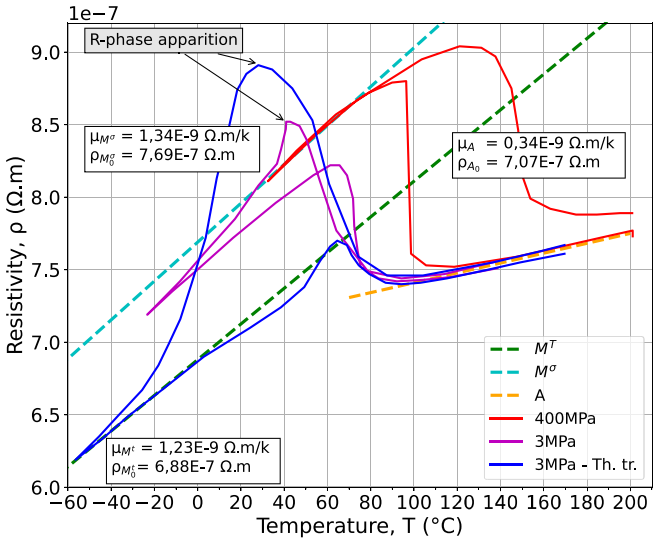

Figure 7. DN resistivity diagram.

an almost pure thermally-induced martensite, stress-induced martensite or austenite. The non-linear stages (transient state) reveal the phase transformation process.

As mentioned in the previous section, the *R*-phase can also be present in the wires' microstructure. The apparition of the *R*-phase is very prominent in the resistivity diagram due to its higher electric resistivity value and thus easy to identify in certain conditions, as indicated by the arrows in figures 7 and 8. For the studied wires, the $A \longleftrightarrow R$ and the $R \longrightarrow M^\sigma/M^T$ phase transformations can take place. The conditions in which they occur are estimated by using the resistivity measurements and the temperature-stress slope (C_R) as 20 MPa/°C, based on the literature ([22, 33, 37, 38]), and they are indicated by a darker zone on the phase diagrams (figures 5 and 6).

It is worth noting that the curves signaled as 'Th. tr' denote thermally treated. In fact, due to the accumulation of internal stress in training process, the trained wires (in this case, the

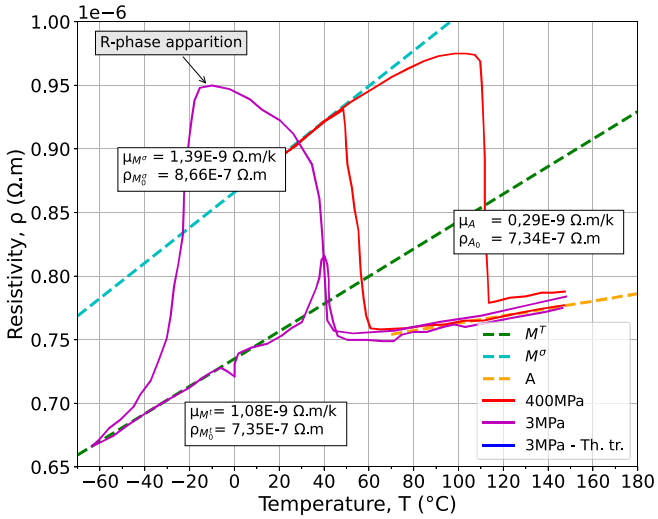

Figure 8. FW resistivity diagram.

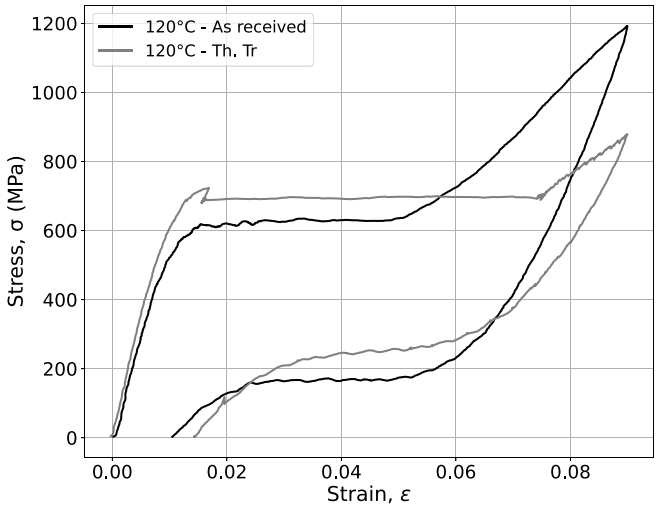

Figure 9. Comparison between as received and 'Th. tr.' DN wire at 120 °C.

DN) do not show a thermally-induced pure state in any thermo-mechanical condition. So, in order to achieve this pure state for the phase proportioning calculation, a mild and short tempering process with maximum temperature of 250 °C (value far from the melting point or aging treatment temperatures [27]) was performed.

In figure 7, one can note that the resistivity evolution for the pure austenite phase is the same for the Th. tr. and as received DN wire. In addition, the stress vs. strain response (figure 9) shows the typical slight difference between trained and as built SMAs [29]. Thus, in this case, the employed procedure can be seen as a thermal flash, used to eliminate the residual martensite from the material, that does not change considerably the microstructural state [39, 40].

Once the thermomechanical and electrical properties are acquired, the analysis of the MT/DT kinetics and the influence of the plasticity on resistivity measures can be performed. In

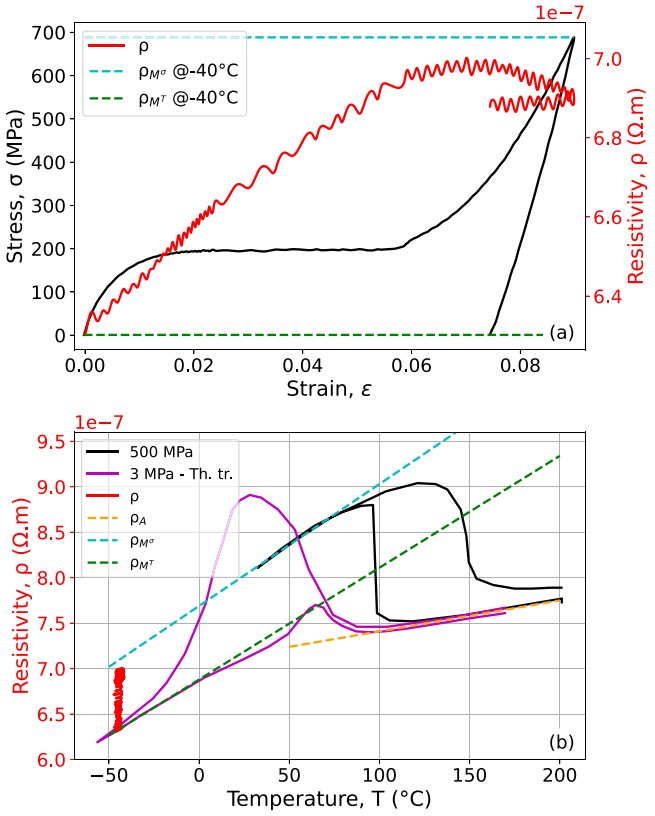

Figure 10. Stress\ resistivity vs. strain (a) and resistivity vs. temperature (b) for an isothermal loading at −40 °C—DN wire.

the next sections, phase proportioning methods will be used in order to observe each of those phenomena in the material.

3.2. *Results of two-state phase proportioning*

After post-processing of acquired test data, the obtained results are plotted in two different figures for each loading.

First, a PP loading was performed (figures 10–13). By observing only the stress vs. strain response, the behavior seems to agree with the standard SMA-response based on literature experimental curves [1, 2, 28]

Typically, the end of SP (strain plateau) is associated with the end of phase transformation or reorientation. Meanwhile, when the resistivity is observed, it shows an increase before and after the SP section. The same pattern is observed by analyzing the z_{M^σ} evolution in figures 11(b) and 13(b).

This behavior indicates that after the phase transformation/reorientation takes place (SP section), other microstructural motions occur. Similar analyses performed in NiTi by [41, 42] are in agreement with these observations and show that this microstructural rearrangement corresponds to a twinning mode in martensite of (001) type (also called compound twin) during PP loading. Besides, in figure 13(b), the relation between z_{M^σ} and ε^{tr} is almost linear until the end of the SP and then, a slope lower than $1/\gamma$ is achieved. This highlights the fact that after the SP, a different kinetics evolution takes place due to the multi-stage character of the martensite reorientation. This change of kinetics can be associated with an intrinsic NiTi

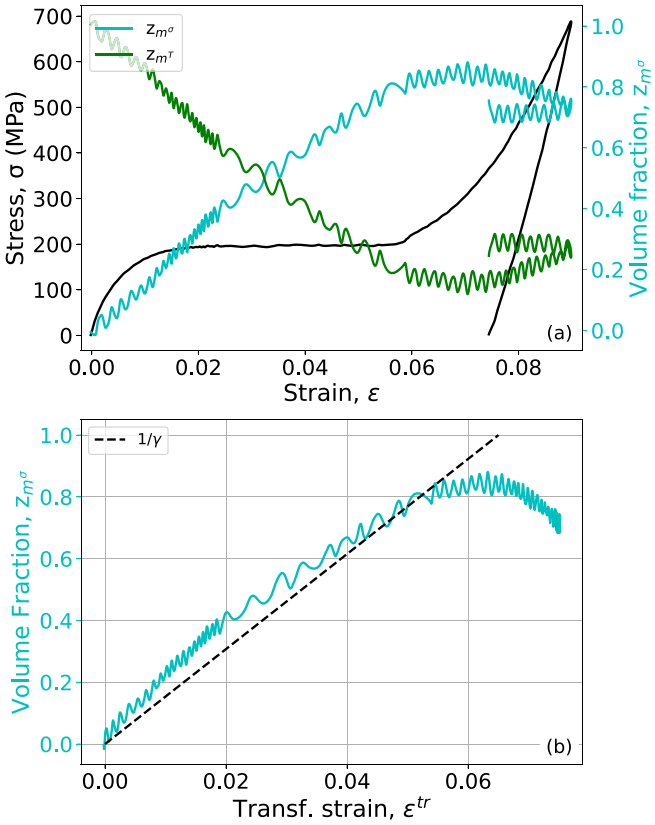

Figure 11. Stress\ volume fraction vs. strain (a) and volume fraction vs. transf. strain (b) for an isothermal loading at −40 °C—DN wire.

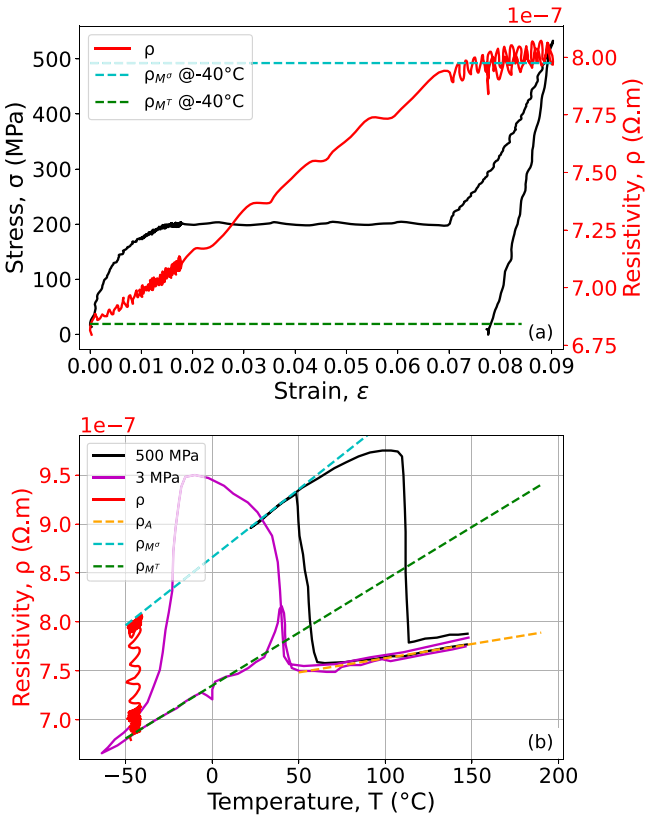

Figure 12. Stress\ resistivity vs. strain (a) and resistivity vs. temperature (b) for an isothermal loading at −40 °C—FW wire.

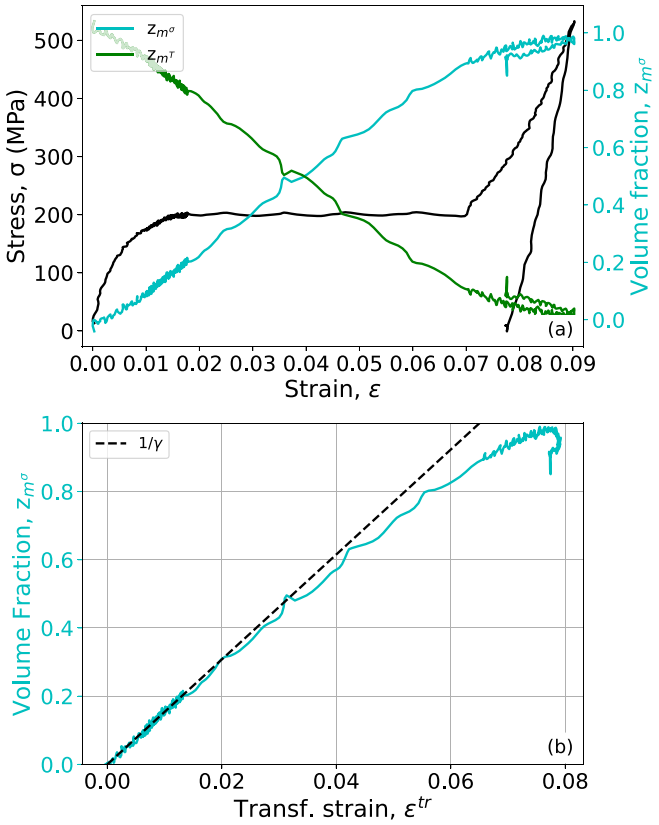

Figure 13. Stress\ volume fraction vs. strain (a) and volume fraction vs. transf. strain (b) for an isothermal loading at −40 °C—FW wire.

characteristic and plastic effects, originated from high-stress levels or training processes. Independently fromits origin, a non negligible difference between the supposed linear evolution between z_{M^σ} and ε^{tr} and the kinetic of MT/DT of this material is observed. This discrepancy can have an unfavorable effect on modeling and design aspects since, by default, this linear relationship is employed in NiTi SMAs.

In the next sections, the impact of this assumption will be evaluated and then the influence of the elastic and plastic strain on the resistivity measurements will also be clarified.

3.3. Results of three-state phase proportioning

As it was already described before, a relation between z_{M^σ} and ε^{tr} is required for the three-state phase proportioning processing. By considering the linear relation this approach in NiTi wires, figures 14 and 15 shows the composition of different states during an isothermal loading at 100 °C. When analyzing the evolution of each volume fraction during the loading in figure 15(a), the result shows an unreal composition.

First, at 100 °C no thermally-induced martensite should be present in the wire, as it can be checked in the phase diagram (figure 5) and yet, an amount of ±15% is reached at 6% of load. Moreover, negative values for z_{M^T} are indicated. In addition, negative values for z_{M^T} are obtained, where they are inconsistent with a real condition.

Tests using the same method were carried out in FW wires and at other thermomechanical conditions and similar results were obtained. It can therefore be deduced that equation (19) shows some limitations for this type of alloy and that its adoption may lead to erroneous results when designing NiTi based structures

3.4. Elasticity influence on electric resistivity

Once the limits of the MT/DT and the phase proportioning methods are evaluated, the next step is to determine the influence of the elastic and plastic strain on the resistivity measurements. First, an isothermal loading-unloading path (0 MPa → 400 MPa → 0 MPa → start of MT) is proposed to analyze elasticity effect on electric resistivity. The results of loading in both wires are presented in figures 16–19.

For stress values below 400 MPa, the wires behave elastically and in this zone the resistivity does not evolve considerably. Then, for higher stress values the resistivity starts to rise, indicating the beginning of MT or apparition of M^σ, before the SP zone, as already mentioned. Thus, one can consider $\partial\rho_A/\partial\varepsilon^{\text{el}} = 0$.

Then, to evaluate the relations $\partial\rho_{M^T}/\partial\varepsilon^{\text{el}}$ and $\partial\rho_{M^\sigma}/\partial\varepsilon^{\text{el}}$, some tests were performed, but no conclusive results on the irrelevancy of elastic deformation on the variation of resistivity in the M^T or M^σ state were obtained. In fact, since the MT/DT starts and ends in the surroundings of the SP, a pure elastic state will only appear in a very narrow window at low temperatures. So, in these conditions, it is not possible to differentiate whether or not there is an influence of the elasticity. Based on

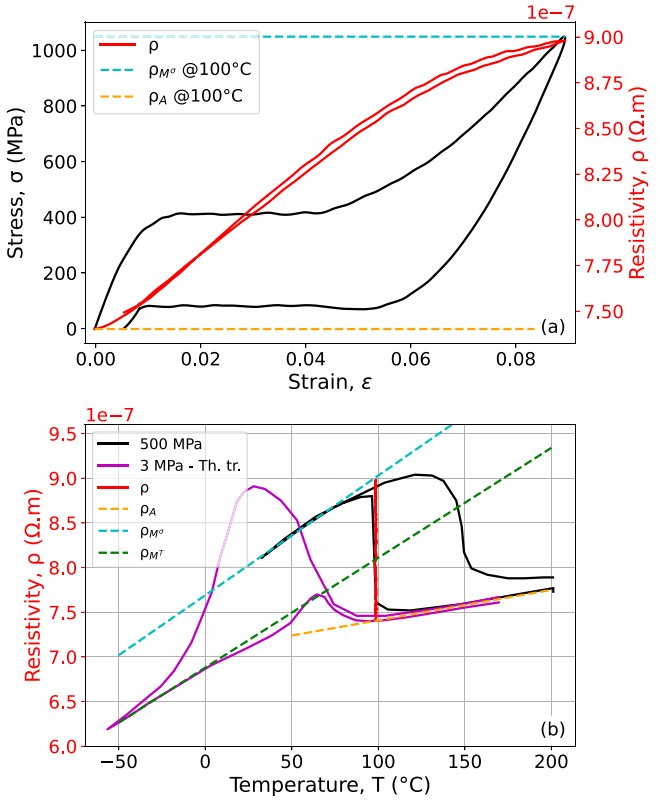

Figure 14. Stress\ resistivity vs. strain (a) and resistivity vs. temperature (b) for an isothermal loading at 100 °C—DN wire.

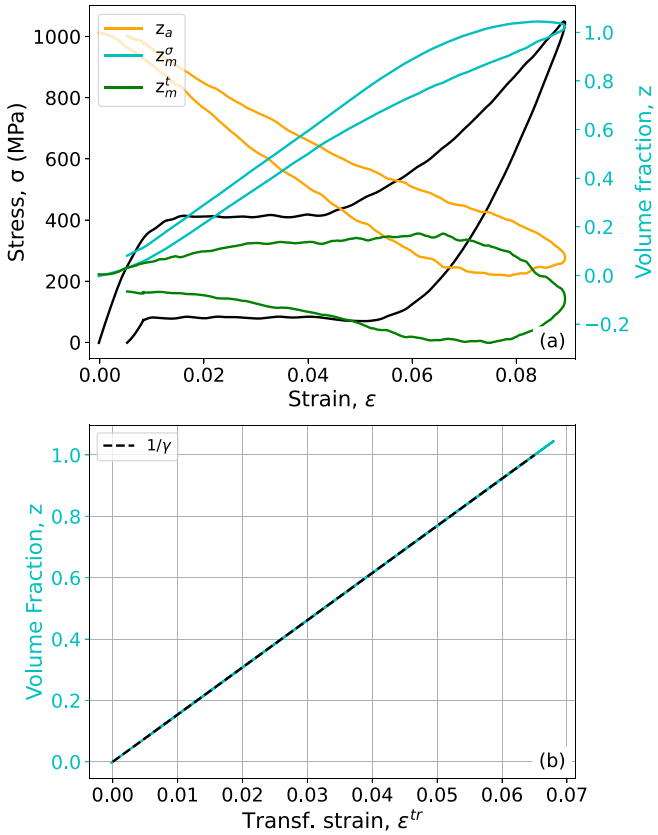

Figure 15. Stress\ volume fraction vs. strain (a) and volume fraction vs. transf. strain (b) for an isothermal loading at 100 °C—DN wire.

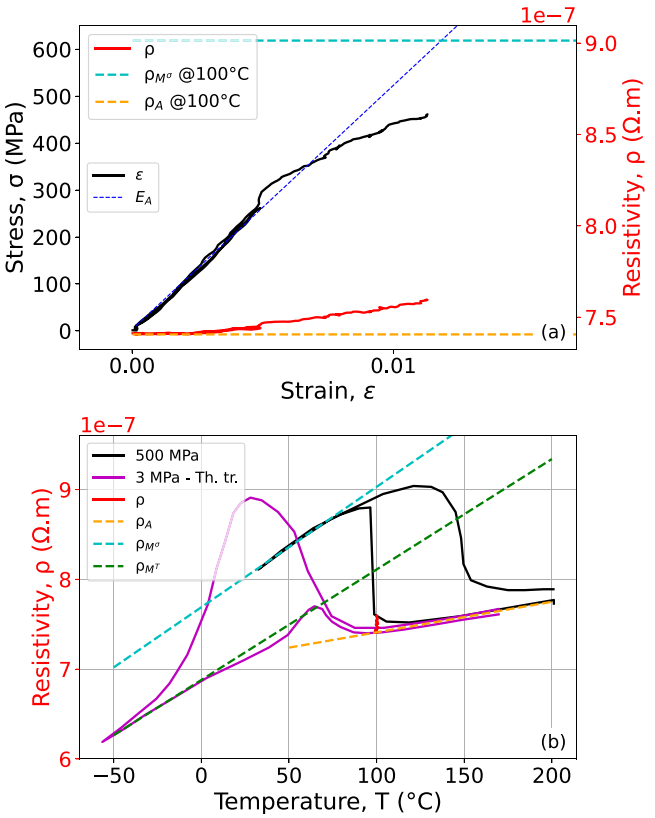

Figure 16. Stress\ resistivity vs. strain (a) and resistivity vs. temperature (b) for an isothermal loading at 100 °C—DN wire.

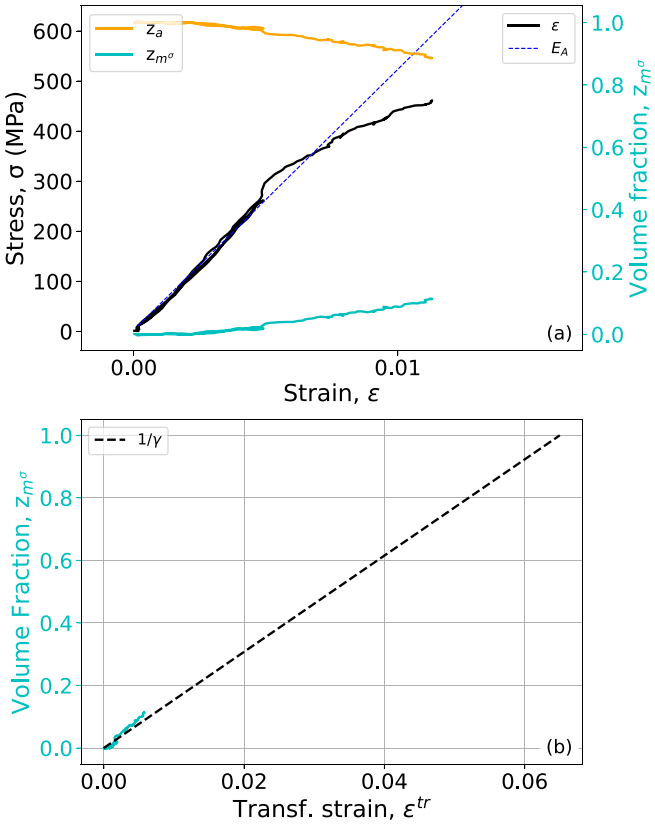

Figure 17. Stress\ resistivity vs. strain (a) and resistivity vs. temperature (b) for an isothermal loading at 100 °C—DN wire.

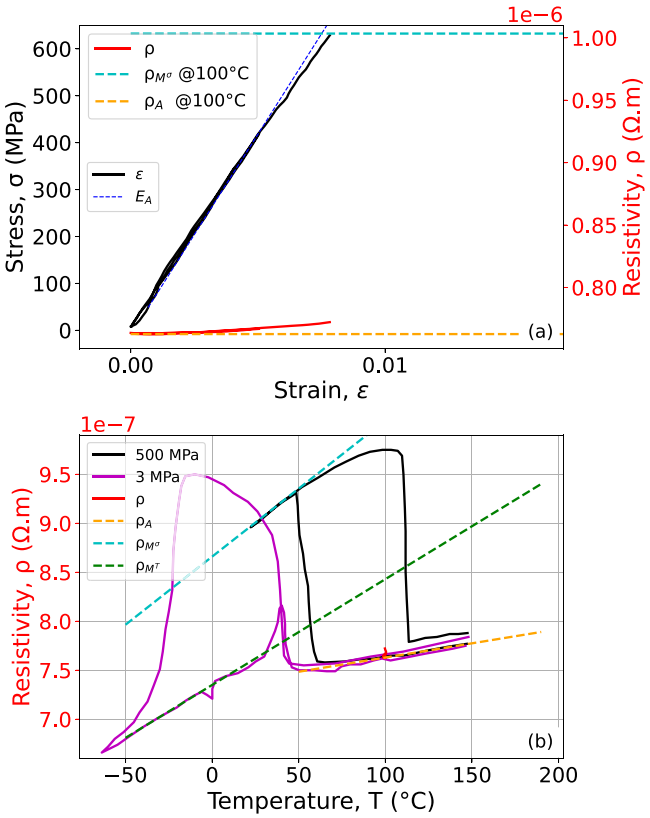

Figure 18. Stress\ resistivity vs. strain (a) and resistivity vs. temperature (b) for an isothermal loading at 100 °C—FW wire.

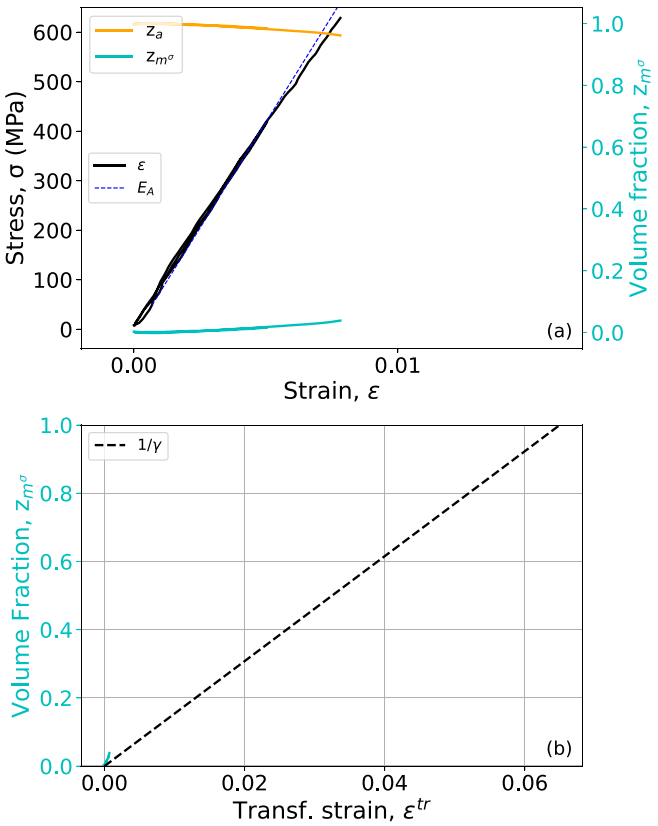

Figure 19. Stress\ resistivity vs. strain (a) and resistivity vs. temperature (b) for an isothermal loading at 100 °C—FW wire.

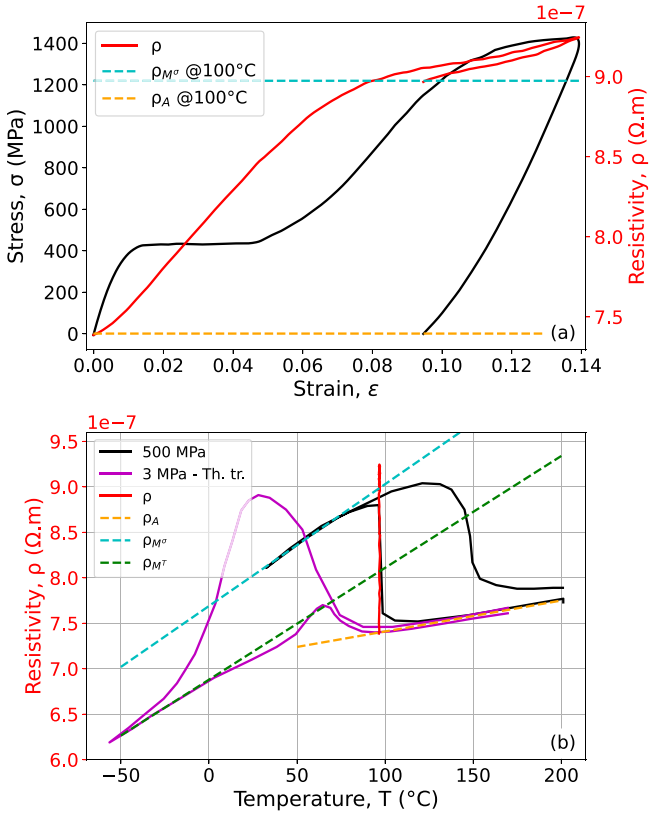

Figure 20. Stress\ resistivity vs. strain (a) and resistivity vs. temperature (b) for an isothermal loading at 100 °C—DN wire.

the results for austenite phase and on other observations from the literature ([32]), the resistivity of all phases will be considered independent from the elastic strain.

3.5. *Plasticity influence on electric resistivity*

To investigate the impact of plastic strains, observations during PP and SE loading for both wires were performed.

First, when comparing figures 10 and 12, a considerable difference on resistivity evolution can be observed, especially in the zone with higher strain values. At this state, the wire is subjected to higher stress condition, triggering the apparition of dislocation slips [5, 8, 43].

Furthermore, for the FW wire, the resistivity increases very little after the end of the SP while for the DN one, the resistivity decreases. This difference between the two responses can be associated with the interaction between plasticity and DT. In this case, as the DN wire was subjected to training, it has more accumulated dislocations than the FW one and when the loading evolves to a higher stress zone, the impact of plasticity is more pronounced.

By examining the impact of plasticity in figure 10(a), one can observe that z_{M^σ} rises until 7% of deformation, and then it starts decreasing. This reduction would take place only in case of reverse phase transformation, but this condition is possible considering the loading history. Then, it can be inferred that plasticity mechanisms are responsible for this apparent reduction of the stress-induced martensite volume fraction, so the resistivity of the stress-induced martensite depends on the interaction between plasticity and martensite transformation.

In order to highlight the effect of plasticity in resistivity measurements, two last tests were performed in a severe stress condition for the DN wire. Figures 20 and 21 show the result for an imposed 14% strain on a DN wire. It can be noted that the maximum stress achieved was about 1400 MPa, a value probably beyond the elastic limit of the material. Then, for the stress vs. strain curve, the evolution of z_{M^σ} corresponds to the occurrence of plasticity mechanisms in two different moments. First, during the effective phase transformation, dislocation slips are probably triggered by transformation-induced plasticity mechanisms [8, 30, 44, 45], which is linked to the change in the slope of the z^{M^σ} evolution. Second, when the phase transformation is finished, the twinning-induced plasticity becomes the major actor, which is responsible for the abrupt change of $z_{M^\sigma}/\varepsilon^{tr}$ relation and for the z_{M^σ} value beyond 1 [10, 11, 46].

Furthermore, the resistivity curve shows again an incompatible evolution with the presented loading in figure 21, increasing over the maximum possible value of (resistivity for the full stress-induced martensite). In this case, the main cause for the exceedance of the z_{M^σ} and ρ_{M^σ} values is the plasticity, the only additional effect introduced in the loading, when compared to the same loading performed in figure 14. The same pattern can also be seen in the thermomechanical loading in figures 22 and 23. For this loading the plasticity mechanisms are more pronounced during the reverse transformation.

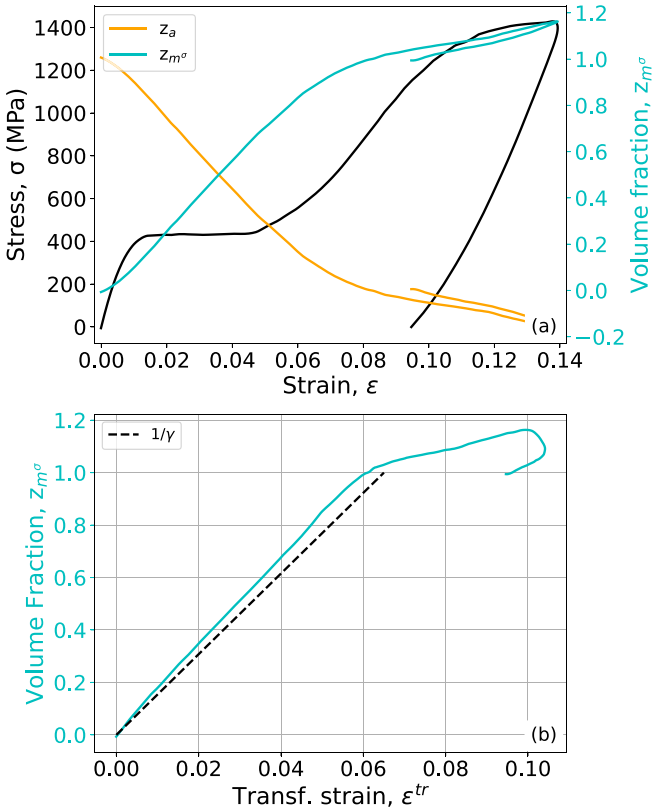

Figure 21. Stress\ volume fraction vs. strain (a) and volume fraction vs. transf. strain (b) for an isothermal loading at 100 °C—DN wire.

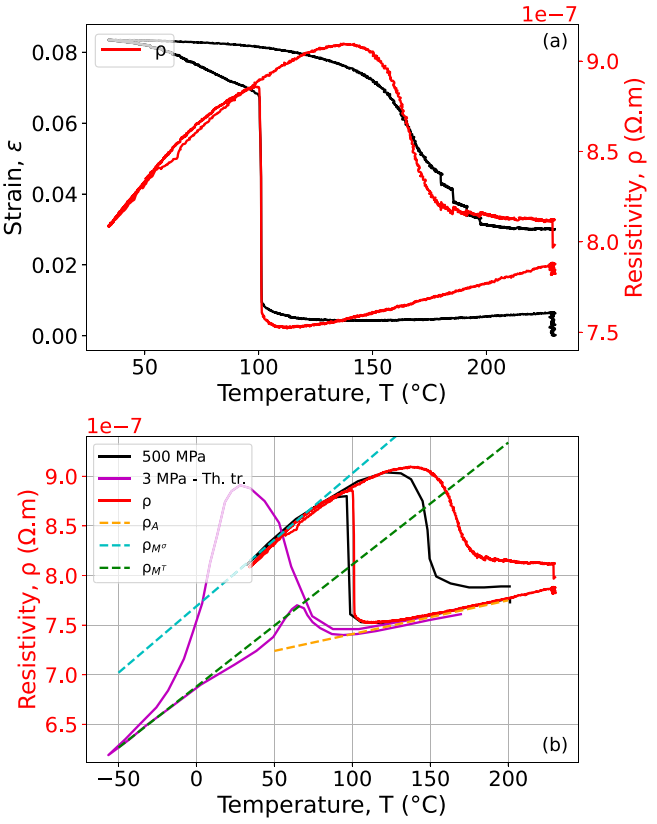

Figure 22. Strain\ resistivity vs. temperature (a) and resistivity vs. temperature (b) for an anisothermal loading at 600 MPa—DN wire.

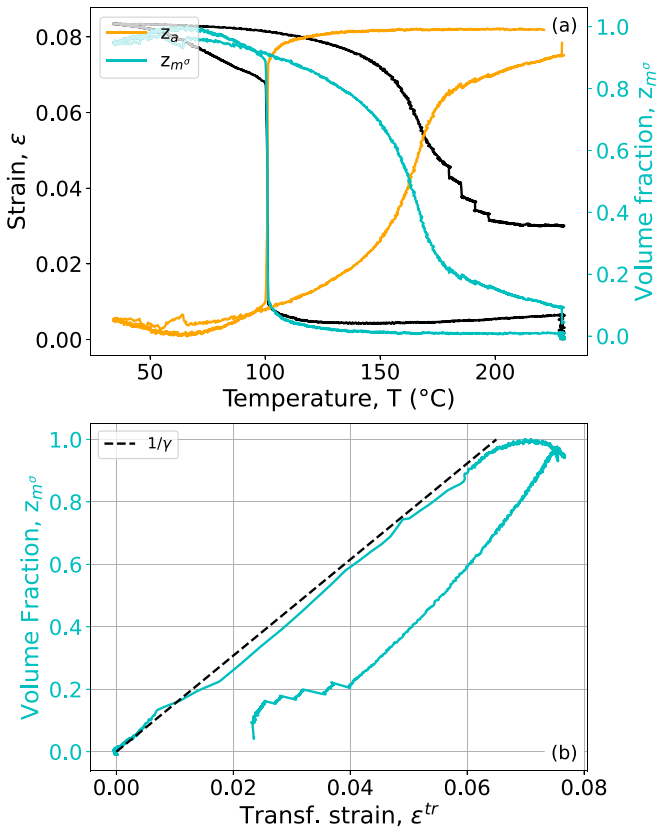

Figure 23. Strain\ volume fraction vs. temperature (a) and volume fraction vs. transf. strain (b) for an anisothermal loading at 600 MPa—DN wire.

Two other relations remain to be defined ($\partial\rho_{M^T}/\partial\varepsilon^p$ and $\partial\rho_A/\partial\varepsilon^p$). However, they are harder to be highlighted by conventional testing conditions. The occurrence of thermally-induced martensite associated with plastic strain is possible but unlikely, because the twinned martensite will detwin and transform into stress-induced martensite before reaching higher stress values (when the plasticity would appear). Still, a comparison between two different microstructural states (with and without dislocations) could be performed in order to indirectly evaluate the impact of the ε^p, but this mentioned experiment was not performed in this work, thus, the first mentioned relation still remains to be evaluated. For the second relation, the possible impact of the plasticity on the austenite phase will be only possible under severe temperature condition, approaching to unusable operating conditions for SE and SME SMAs. So, it is as well considered non-influent in this analysis.

Finally, one can say that one of the responsible factors for the difference between the supposed linear evolution of $z_{M^\sigma}/\varepsilon^{\mathrm{tr}}$ and the found results for the NiTi alloy is the plasticity.

4. Conclusion

In order to study the kinetics of the phase transformation as well as the impact of plasticity on the thermomechanical behavior of NiTi wires, phase proportioning methods based on electric resistivity measurements were employed.

At first, the performed experiments demonstrated that for this material, a multi-stage reorientation of the martensite can take place during pseudoelastic loading. This suggests that, contrary to the employed linear relation that supposed a single microstructure motion, a different kinetics evolution can occur.

Then, it is evidenced that the plasticity affects the relation between martensite volume fraction and transformation strain. Meanwhile, results show that plastic strain and its accumulation via training effects change considerably the supposed linear relation. Thus, tasks involving this assumption can provide erroneous results as the ones presented with the three-phase proportioning post processing.

In addition, the influence of elasticity and plasticity on resistivity measurements was evaluated. It was revealed that there is no influence on the resistivity of pure phases caused by elastic deformation. However, it was shown that the plastic deformation has a significant impact on the resistivity variations. These results highlight the effect of plasticity on the MT/DT kinetics.

In summary, it can be concluded that the plasticity plays an import role in the kinetics of the MT and DT on NiTi wires, and it can be observed by macroscopic resistivity measurements. Then, a new relation describing this phenomenon must be establish. However, the quantification of this influence was not performed. Further studies on the quantification of the impact of plastic strain on the resistivity is required.

Data availability statement

The data cannot be made publicly available upon publication because they are owned by a third party and the terms of use prevent public distribution. The data that support the findings of this study are available upon reasonable request from the authors.

ORCID iDs

Marcos Lopes Leal Júnior https://orcid.org/0000-0003-4892-1178
Laurent Pino https://orcid.org/0000-0002-8533-5293
Mahmoud Barati https://orcid.org/0000-0003-1928-929X
Laurent Daniel https://orcid.org/0000-0001-5016-4589
Shabnam Arbab Chirani https://orcid.org/0000-0002-8531-8581

References

[1] Rao A, Srinivasa A R and Reddy J N 2015 *Design of Shape Memory Alloy (SMA) Actuators* (*Springer Briefs in Computational Mechanics*) (Springer)
[2] Marfia S and Vigliotti A 2015 1D SMA models *Shape Memory Alloy Engineering* (Boston, MA: Butterworth-Heinemann) pp 99–140
[3] Leary M, Huang S, Ataalla T, Baxter A and Subic A 2013 *Mater. Des.* **43** 460–6

[4] Fumagalli M, Butera F and Coda A 2008 *J. Mater. Eng. Perform.* **18** 691–5
[5] Sedmák P, Šittner P, Pilch J and Curfs C 2015 *Acta Mater.* **94** 257–70
[6] Delville R, Malard B, Pilch J, Sittner P and Schryvers D 2011 *Int. J. Plast.* **27** 282–97
[7] Gao Y, Casalena L, Bowers M, Noebe R, Mills M and Wang Y 2017 *Acta Mater.* **126** 389–400
[8] Šittner P, Sedlák P, Seiner H, Sedmák P, Pilch J, Delville R, Heller L and Kadeřávek L 2018 *Prog. Mater. Sci.* **98** 249–98
[9] Heller L, Šittner P, Sedlák P, Seiner H, Tyc O, Kadeřávek L, Sedmák P and Vronka M 2019 *Int. J. Plast.* **116** 232–64
[10] Bian X, Heller L, Kadeřáve L and Šittner P 2022 *Appl. Mater. Today* **26** 101378
[11] Iaparova E, Heller L, Tuc O and Sittner P 2023 *Acta Mater.* **242** 118477
[12] Alberto P and Savi M 2006 *Math. Probl. Eng.* **2006** 056876
[13] Cisse C, Zaki W and Ben Zineb T 2016 *Int. J. Plast.* **76** 244–84
[14] Mirzaeifar R, Gall K, Zhu T, Yavari A and DesRoches R 2014 *J. Appl. Phys.* **115** 194307
[15] Xu B, Kang G, Kan Q, Yu C and Xie X 2020 *Int. J. Mech. Sci.* **168** 105303
[16] Tyc O, Heller L, Vronka M and Šittner P 2020 *Int. J. Fatigue* **134** 105470
[17] Barati M, Chirani S A, Kadkhodaei M, Saint-Sulpice L and Calloch S 2017 *Smart Mater. Struct.* **26** 025024
[18] Gédouin P A, Chirani S A and Calloch S 2010 *Int. J. Plast.* **26** 258–72
[19] Novák V, Šittner P, Dayananda G N, Braz-Fernandes F M and Mahesh K K 2008 *Mater. Sci. Eng.* A **481–482** 127–33
[20] Barta S, Dieška P, Bielek J, Šmida T and Magula V 2005 *Acta Mater.* **53** 3511–5
[21] Uchil J, Mahesh K K and Kumara K G 2002 *Physica* B **324** 419–28
[22] Urbina C, De la Flor S and Ferrando F 2009 *Mater. Sci. Eng.* A **501** 197–206
[23] Brammajyosula R, Buravalla V and Khandelwal A 2011 *Smart Mater. Struct.* **20** 035015
[24] Zhang J J, Yin Y H and Zhu J Y 2013 *Sensors* **13** 12958–74
[25] Antonucci V, Faiella G, Giordano M, Mennella F and Nicolais L 2007 *Thermochim. Acta* **462** 64–69
[26] Taillard K, Chirani S A, Calloch S and Lexcellent C 2008 *Mech. Mater.* **40** 151–70
[27] Otsuka K and Ren X 2005 *Prog. Mater. Sci.* **50** 511–678
[28] Kumar P and Lagoudas D 2008 Introduction to Shape Memory Alloys *Shape Memory Alloys: Modeling and Engineering Applications* (Boston, MA: Springer) pp 1–51
[29] Urbina C, De la Flor S and Ferrando F 2010 *J. Alloys Compd.* **490** 499–507
[30] Atli K C, Franco B E, Karaman I, Gaydosh D and Noebe R D 2013 *Mater. Sci. Eng.* A **574** 9–16
[31] Wada K and Liu Y 2008 *Mater. Sci. Eng.* A **481–482** 166–9
[32] Saint-Sulpice L, Lakrit M, Arbab Chirani S and Calloch S 2014 *Mech. Mater.* **71** 1–9
[33] Šittner P, Landa M, Lukáš P and Novák V 2006 *Mech. Mater.* **38** 475–92
[34] Zhou T, Yu C, Kang G, Kan Q and Fang D 2020 *Int. J. Solids Struct.* **193–194** 503–26
[35] Juhász L, Schnack E, Hesebeck O and Andrae H 2002 *J. Intell. Mater. Syst. Struct.* **13** 825–36
[36] Helm D and Haupt P 2003 *Int. J. Solids Struct.* **40** 827–49
[37] Helbert G, Saint-Sulpice L, Chirani S A, Dieng L, Lecompte T, Calloch S and Pilvin P 2016 *Smart Mater. Struct.* **26** 025007
[38] Wang L, Feng P, Xing X, Wu Y and Liu Z 2021 *J. Alloys Compd.* **868** 159192
[39] Moreau F 1998 Etude par diffraction des rayons x des effets du cyclage pseudo-élastique de l'alliage á mémoire de forme Cu-Al-Be *These de doctorat Metz* (available at: www.theses.fr/1998METZ011S)
[40] Saint-Sulpice L, Chirani S A and Calloch S 2008 *Mater. Sci. Eng.* A **481–482** 174–7
[41] Molnárová O, Tyc O, Heller L, Seiner H and Šittner P 2021 *Acta Mater.* **218** 117166
[42] Chowdhury P and Sehitoglu H 2017 *Prog. Mater. Sci.* **88** 49–88
[43] Heller L, Seiner H, Šittner P, Sedlák P, Tyc O and Kadeřávek L 2018 *Int. J. Plast.* **111** 53–71
[44] Xiao Y, Zeng P and Lei L 2015 *Smart Mater. Struct.* **25** 017002
[45] Zhang Y, Moumni Z, You Y, Zhang W, Zhu J and Anlas G 2019 *Int. J. Plast.* **115** 307–29
[46] You Y, Wang J, Su X, Guo X, Moumni Z and Zhang W 2020 *Mater. Today Commun.* **24** 101137